Chain Folding in Semicrystalline Oxyethylene/Oxybutylene Diblock Copolymers

Shao-Min Mai,*,† J. Patrick A. Fairclough,‡ Kyriakos Viras,§ Peter A. Gorry,† Ian W. Hamley,|| Anthony J. Ryan,‡,⊥ and Colin Booth†

Department of Chemistry, University of Manchester, Manchester M13 9PL, U.K., Department of Chemistry, University of Sheffield, Sheffield S3 7UF, U.K., Physical Chemistry Laboratory, Department of Chemistry, National and Kapodistrian University of Athens, Panepistimiopolis, 157 71 Athens, Greece, School of Chemistry, University of Leeds, Leeds LS2 9JT, U.K., and CCLRC Daresbury Laboratory, Warrington, WA4 4AD, U.K.

Received July 31, 1997; Revised Manuscript Received October 20, 1997[⊗]

ABSTRACT: The chain folding behavior of oxyethylene/oxybutylene (E/B) diblock copolymers, with one crystallizable E block and one noncrystallizable B block, has been studied by simultaneous SAXS and WAXS, low-frequency Raman spectroscopy, and differential scanning calorimetry. Two models, normal density (ND) and crystal/liquid-crystal (CLC) models were used to explore the results, consideration being given to the difference in the cross-sectional area of the two chains and the need to fill space at approximately normal density. It was found that both models can describe the data for the longer copolymers, but the CLC model is better for the shorter copolymers.

1. Introduction

Diblock copolymers of ethylene oxide and 1,2-butylene oxide, here denoted E_mB_n [E = oxyethylene, OCH_2CH_2, and B = oxybutylene, $OCH_2CH(C_2H_5)$], prepared by sequential anionic copolymerization, have one crystallizable E block and one noncrystallizable B block, this last reflecting the atactic configuration of the B block. Our purpose in this paper is to report lamellar spacings, LAM frequencies, and thermal properties for 22 copolymers in the molar mass range M_n = 2300 to 12500 g mol^{-1}. These results, combined with those from an earlier study of E_mB_n copolymers of comparatively low molar mass, M_n < 3310 g mol^{-1},[1] throw some light on the state of chain folding in the semicrystalline materials. A preliminary report concentrating on three of the copolymers has been published[2] and is referred to herein.

Considering first copolymers with short blocks, unfolded E blocks crystallize into lamellar crystals, and the noncrystalline B blocks are also constrained to an unfolded conformation. This was demonstrated experimentally by combination of small-angle X-ray scattering (SAXS) and low-frequency Raman spectroscopy (LFRS) to study the series of block copolymers $E_{30}B_n$, n < 20.[1] Similar results were obtained for a related series of diblock copolymers $E_{40}P_n$, n < 11 [P = oxypropylene, $OCH_2CH(CH_3)$].[3] However, and more interestingly, it was shown[1] that the unfolded conformation of the $E_{30}B_n$ copolymers became unstable if the B-block length was increased to 30 units; i.e., in crystalline $E_{31}B_{30}$ the E block was folded once and the B block was unfolded. This effect was judged to be a direct result of the difference in cross-sectional area of the two chains (E_m, 21 Å^2; B_n, 34 Å^2) coupled with the need to fill space at approximately normal density.[1]

Considering lengthy copolymers, published theories[4−6] recognize a competition between preferred low-Gibbs-energy conformations of the two blocks, i.e., unfolded chains for the crystallized component and randomly-coiled chains for the noncrystallized component, and minimize the Gibbs energy by introducing an equilibrium degree of chain folding in the crystalline layer. Not surprisingly, experimental studies of corresponding systems, i.e., fairly high molar mass block copolymers with mobile noncrystalline components, have shown chain folding to be the norm.[7−13]

There is an important distinction to be drawn between homopolymers in which chain folds are metastable, induced by rate effects, and block copolymers where an equilibrium degree of chain folding exists in the crystalline layer. In practice with lengthy copolymers it is difficult to separate the kinetic and thermodynamic effects. With short copolymers, as studied previously,[1] thermodynamic effects predominate. The range of copolymers studied in this work take us from the region of predominantly thermodynamic control towards the region where kinetic control becomes important and equilibrium folded structures can be achieved only by very carefully controlled crystallization.[2]

The copolymers were designed primarily to suit investigations of their structures in the melt state, some of which have been described already,[1,14] and not for a systematic investigation of their crystallization and crystallinity. Nevertheless, the E_mB_n copolymers prepared enabled these properties to be sampled over a wide range of molar mass and composition, thus yielding new results of considerable interest.

2. Experimental Section

2.1. Materials. The methods used in the synthesis of the copolymers by sequential anionic polymerization and their characterization by GPC and NMR have been described previously.[1,14] All copolymers were of low polydispersity (M_n/M_w < 1.05) and all were at least 99 wt % diblock copolymer, the impurity (if any) being a small fraction of triblock copolymer generated from difunctional poly(oxyethylene) initiated by adventitious moisture in the first stage of copolymerization. Formulas (see Table 1) are quoted as E_mB_n, where m and n are number-average block lengths in E and B units respectively, known to ±1%. Also given in Table 1 are the weight fraction of oxyethylene in the copolymer (w_E), the volume fraction of oxyethylene in the crystalline copolymer

† University of Manchester.
‡ University of Sheffield.
§ National and Kapodistrian University of Athens.
|| University of Leeds.
⊥ CCLRC Daresbury Laboratory.
⊗ Abstract published in *Advance ACS Abstracts,* December 1, 1997.

S0024-9297(97)01158-3 CCC: $14.00

Table 1. Oxyethylene/Oxybutylene Diblock Copolymers[a]

copolymer	w_E (solid state)	ϕ_E (solid state)	liquid-state structure	liquid-state d/Å (70 °C)
$E_{35}B_{12}$	0.64	0.58	dis	
$E_{36}B_{18}$	0.55	0.49	dis	
$E_{43}B_{23}$	0.53	0.47	dis	
$E_{47}B_{62}$	0.32	0.27	hex	104
$E_{49}B_{9}$	0.77	0.72	dis	
$E_{56}B_{27}$	0.56	0.50	lam	89 (50 °C)
$E_{60}B_{29}$	0.56	0.50	lam	93 (50 °C)
$E_{64}B_{60}$	0.40	0.34	hex	119
$E_{68}B_{65}$	0.39	0.34	hex	126
$E_{70}B_{69}$[b]	0.40	0.32	hex	136
$E_{75}B_{54}$	0.46	0.40	$Ia\bar{3}d$	123
$E_{76}B_{38}$	0.55	0.49	lam	109
$E_{85}B_{45}$	0.54	0.48	lam	119
$E_{96}B_{47}$	0.56	0.50	lam	127
$E_{100}B_{51}$	0.55	0.49	lam	131
$E_{110}B_{30}$	0.69	0.64	lam	115
$E_{114}B_{56}$	0.55	0.50	lam	146
$E_{115}B_{103}$	0.41	0.35	hex	177
$E_{131}B_{35}$	0.70	0.64	lam	138
$E_{134}B_{19}$	0.81	0.77	dis	
$E_{155}B_{76}$	0.56	0.50	lam	174
$E_{209}B_{45}$	0.74	0.69	lam	180

[a] $w_E = n/[n + (72/44)m]$. $\phi_E = n/[n + (72/44)(1.23/0.97)m]$, 1.23 g cm^{-3} being the density of poly(oxyethylene) in the crystalline state and 0.97 g cm^{-3} the density of poly(oxybutylene) in the liquid state, both at 20 °C. dis = disordered; lam = lamella; hex = hexagonal (packed cylinders); $Ia\bar{3}d$ = bicontinuous cubic phase. [b] Sample with deuterated E block: $w_E = n/[n + (72/48)m]$.

(ϕ_E), and the liquid-state structure and its d spacing determined by SAXS as described elsewhere.[14]

2.2. Time-Resolved X-ray Scattering. Measurements were made on beamline 8.2 of the SRS at the CCLRC Daresbury Laboratory, Warrington, U.K.[15] The camera was equipped with a multiwire quadrant detector (SAXS) located 3.5 m from the sample position and a curved knife-edge detector (WAXS) that covered 70° of arc at a radius of 0.3 m. Samples were placed in a TA Instruments DSC pan containing a 0.75 mm brass spacer ring and fitted with windows made from 25 μm thick mica. The loaded pans were placed in the cell of a Linkam DSC of single-pan design. A complete description of the DSC and the sample pans, including calibration of the temperature scale, can be found elsewhere.[16,17] The temperature program was varied, depending on the sample under investigation, as described in section 2.5.

The scattering pattern from an oriented specimen of wet collagen (rat-tail tendon) was used to calibrate the SAXS detector, and high-density polyethylene, aluminum, and an NBS silicon standard were used to calibrate the WAXS detector. Parallel plate ionization detectors placed before and after the sample cell recorded the incident and transmitted intensity. The data acquisition system[17] had a time-frame generator which collected the SAXS/WAXS data in 6 s frames separated by a wait-time of 10 μs. The experimental data were corrected for background scattering (subtraction of the scattering from the camera, hot stage, and an empty cell), for sample thickness and transmission, and for any departure from positional linearity of the detectors.[18]

Polycrystalline solids with small domains relative to the sample size can be isotropic with respect to the X-ray pattern: i.e., all orientations can be adequately sampled in a one-dimensional experiment. In fact, replicate crystallizations of the present samples gave different intensities of reflections relative to one another, indicating some orientation in the thin films. For present purposes this effect was unimportant.

2.3. Raman Spectroscopy. Raman scattering at 90° to the incident beam was recorded by means of a Spex Ramalog spectrometer fitted with a 1403 double monochromator plus a third (1442U) monochromator operated in scanning mode. The light source was a Coherent Innova 90 argon-ion laser operated at 514.5 nm and 500 mW. Typical operating conditions were as follows: low-frequency range, bandwidth 0.8 cm^{-1}, scanning increment 0.05 cm^{-1}, integration time 6−12 s; high-frequency range, bandwidth 2 cm^{-1}, scanning increment 1 cm^{-1}, integration time 4 s. The low-frequency scale was calibrated by reference to the 9.4 and 14.9 cm^{-1} bands in the spectrum of L-cystine.

Samples, crystallized as described in section 2.5, were mounted in the hollowed end of a stainless-steel rod so as to form a plane surface. Spectra were recorded with the samples at room temperature, i.e., approximately 20 °C. Precise control of temperature was not sought, as the temperature derivative of frequency was known to be small for the LAM-1 bands of poly(oxyethylene).[19]

2.4. Differential Scanning Calorimetry. A Perkin-Elmer DSC-4 was used. Samples of the copolymers (*ca.* 5 mg) sealed into aluminum pans were prepared as described in section 2.5. Heating was from 20−25 °C to a temperature some 15 °C above the melting point of the sample. Heating rates were in the range +2 to +20 °C min^{-1}.

Melting temperatures (T_m) were obtained from the temperatures at the peaks of the endotherms (T_{pk}), and enthalpies of fusion ($\Delta_{fus}H$) were obtained from peak areas *via* a LabVIEW program DSC 1.03. The temperature and power scales of the calorimeter were calibrated by melting indium, and the temperature scale was checked by melting point standards. Thermal lag was determined by melting the standards at different heating rates (r) and linearly extrapolating T_{pk} against $r^{1/2}$ to zero heating rate, i.e., to the true values of T_m. Melting temperatures of the copolymers obtained using different heating rates were in substantial agreement provided that correction was made for thermal lag. As required for a power compensation DSC, enthalpies of fusion were independent of heating rate.

2.5. Crystallization of Samples. Dry samples of the copolymers (*ca.* 5 mg) were taken from storage at −10 °C and, under dry conditions at room temperature, sealed into appropriate DSC pans. The following procedures applied to samples for conventional DSC.

Stored. Samples were taken from storage and examined without further treatment.

Cooled. Samples were heated to 15 °C above their melting temperature (T_m + 15 °C), held for 15 min, and cooled at 10 °C min^{-1} to 20 °C.

Quenched. Samples were heated to 15 °C above their melting temperature (T_m + 15 °C), held for 15 min, cooled as rapidly as possible to 0 °C (approximate cooling rate 100 °C min^{-1}), and held at that temperature for 15 min.

Specified Temperature. Samples were heated to T_m + 15 °C, held for 15 min, quenched to a specified temperature (often T_m − 10 °C), held at that temperature for 12−24 h to complete crystallization, and finally quenched to 20 °C.

Self-Seeded. Crystalline samples were heated at 50 °C min^{-1} to the melting point, held at T_m for 30−60 s, quenched to T_m − 5 °C, held at that temperature for 12−24 h to complete crystallization, and finally quenched to 20 °C.

Samples for Raman spectroscopy were prepared in the DSC-4 exactly as described above, before being transferred to the metal "Raman" cells.

Samples for SAXS/WAXS were prepared in analogous ways but in the modified TA pans: maximum heating and cooling rates were +40 and −60 °C min^{-1}. Prolonged crystallization times were not necessary in the time-resolved experiments.

Certain samples were annealed, the conditions for which are noted when reporting the results.

3. Results and Discussion

3.1. WAXS. WAXS patterns were compared directly with those from crystalline samples of low-molar-mass poly(oxyethylene), and they were found to be essentially identical. An example is shown in Figure 1. All reflections could be indexed to the crystal structure of poly(oxyethylene),[20] i.e., to the monoclinic subcell of the structure with alternating right-hand and left-hand distorted 7/2 helices.

3.2. SAXS. The general features of the SAXS experiments are illustrated in Figure 2 (copolymer

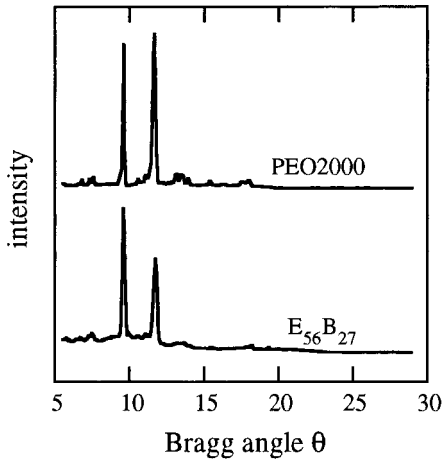

Figure 1. WAXS intensity (arbitrary scale) *vs* Bragg angle (θ) for crystalline copolymer $E_{56}B_{27}$ and poly(ethylene glycol) PEO2000. Wavelength = 1.54 Å.

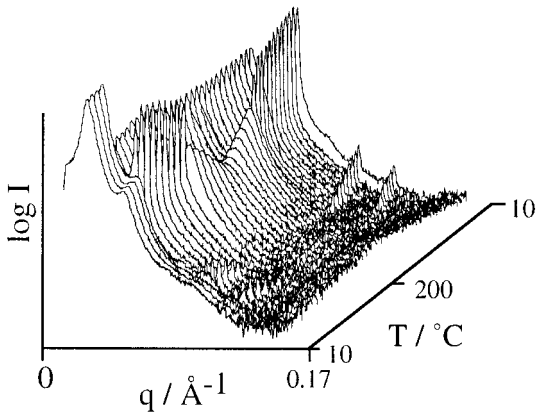

Figure 2. Three-dimensional relief diagram of time-resolved SAXS data obtained during melting and recrystallization of copolymer $E_{68}B_{65}$. The heating cycle was 10 °C → 200 °C → 10 °C at a ramp rate of 10 °C min^{-1}. The plot shows intensity (I, arbitrary logarithmic scale) *vs* scattering vector (q) *vs* temperature (T).

$E_{68}B_{65}$), which shows time-resolved scattering from the lamellar structure of the crystalline copolymer at $T <$ 47 °C, from the hexagonal structure of the ordered melt at 47 < T < 140 °C, and from the disordered melt at T > 140 °C, with the reverse sequence on cooling. Present interest is in scattering from the crystalline copolymer, for which plots of intensity against q (see, for example, Figure 3) were used to calculate the lamellar spacing from the position q^* of the first-order maximum, i.e. $d = 2\pi/q^*$. Here the scattering vector $q = (4\pi/\lambda) \sin \theta$, where λ is the X-ray wavelength and θ is the Bragg angle. Patterns from well-crystallized samples could be fitted with Gaussian functions for the peaks and a smooth Porod background. Because of the narrow peaks, Lorentz correction of the data resulted in insignificant change in d.

Lamellar spacings were obtained for all copolymers in their semicrystalline state: see Table 2. The response to different time−temperature programs was investigated for several copolymers. Figure 4 shows the variation of the dominant spacing with temperature and time for copolymer $E_{64}B_{60}$, which had a hexagonal melt. The sequence of events on slow heating and cooling, fast heating and cooling, and annealing, is clearly seen: melting of the stored sample ($d \approx 230$ Å) to the hexagonal liquid phase ($d \approx 125$ Å), disordering at the ODT, reordering at the DOT, crystallization (slow cooling) to a lamellar crystal phase with $d \approx 170$ Å, fast

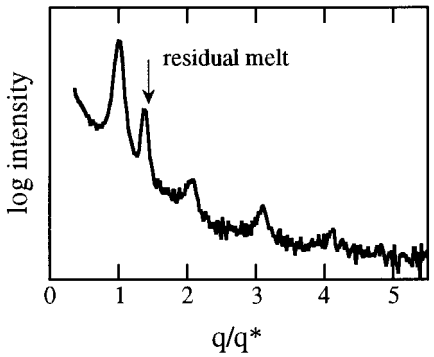

Figure 3. SAXS pattern (20 °C) for copolymer $E_{155}B_{76}$. The plot is log(intensity) (arbitrary scale) *vs* q/q^*, where q^* is the value of q at the first maximum. The first four orders of scattering from the lamellar structure are clearly seen. The peak at $q/q^* \approx 1.4$ is from a residue of the structured melt (hexagonal).

heating followed by quenching to a lamellar crystal phase with $d \approx 130$ Å, essentially identical to d in the melt at low temperature, and finally annealing at 45 °C causing rapid reorganization to a lamellar crystal phase with $d \approx 220$ Å. Similar epitaxial behavior was found for other copolymers with hexagonal melts, e.g. for copolymers $E_{70}B_{69}$ and $E_{115}B_{103}$ as described and discussed previously.[2] Epitaxy (or near epitaxy) between hexagonal melt and quenched lamellar crystal phases has been described for other systems.[13]

Application of a similar time-temperature program to copolymer $E_{75}B_{54}$ ($Ia\bar{3}d$ melt) is illustrated in Figure 5. For this copolymer, the lamellar crystal phase formed on quenching had a d spacing significantly larger (by some 40 Å) than its melt. A similar situation has been illustrated previously for copolymer $E_{76}B_{38}$ which has a lamellar melt.[2] Epitaxy between melt and quenched lamellar crystal phases was found only for those copolymers which had hexagonal melt phases.

The lamellae in most crystals formed by quenching could be thickened by annealing, as seen in Figures 4 and 5, and indicated in Table 2. Annealing for long times at high temperatures was not possible in the SAXS experiments, and it is probable that the equilibrium state was not reached, although the evidence we have is that the rate of lamellar thickening was fast: see Figures 4 and 5. Certainly for the two copolymers for which comparison was made ($E_{85}B_{45}$ and $E_{209}B_{45}$, see Table 2 for details), the d spacings after a period of annealing did not match those obtained by self-seeded crystallization at high temperature.

Two models were used to explore the results, both of which assume poly(oxyethylene) helices with axes normal to the lamellar end plane and with integer numbers (0, 1, 2, etc.) of folds.

Normal Density (ND) Model. For a two-phase model of a lamella with unfolded crystalline E blocks and noncrystalline B blocks at normal density, the lamellar spacing would be

$$d_0/\text{Å} \approx 0.95 z_E/\phi_E \quad (1)$$

where z_E is the number of chain atoms (C and O) in the E block, ϕ_E is the volume fraction of E block in the solid state, and 0.95 Å is the length per chain atom along the oxyethylene helix axis.[21] The calculation of ϕ_E (see Table 1) assumes that the E component is perfectly crystalline, but that is not an essential feature of the model. Keeping the same model, it is a simple matter to estimate the repeat length in a system in which the

Table 2. Lamellar Spacings (SAXS, 25 °C) for Crystalline Oxyethylene/Oxybutylene Diblock Copolymers

		lamellar spacing/Å					
copolymer	T_m/°C	store	cool	quench	$T_c \approx T_m - 10$	self-seeded ($T_c \approx T_m - 5$)	anneal[a]
$E_{35}B_{12}$	43	125	108				
$E_{36}B_{18}$	42	171	138				167 (41 °C)
$E_{43}B_{23}$	46	151	118				
$E_{47}B_{62}$	43	216	155[b]				
$E_{49}B_9$	49	154					
$E_{56}B_{27}$	49	171	139				174 (47 °C)
$E_{60}B_{29}$	50	179	146			197	
$E_{64}B_{60}$	46	233	172	131			217 (45 °C)
$E_{68}B_{65}$	46	225	166	136			236 (47 °C)
$E_{70}B_{69}$[c]				143		253	
$E_{75}B_{54}$	51	214	168	160			237 (49 °C)
$E_{76}B_{38}$	56	188	158		185[d]	224	
$E_{85}B_{45}$	52	200	168	162		264	229 (51 °C)
$E_{96}B_{47}$	58	194	176		194	255	
$E_{100}B_{51}$	53	205	186				
$E_{110}B_{30}$	57	180	159	155		214	
$E_{114}B_{56}$	56	220	198		220	220	
$E_{115}B_{103}$	53	231		188			
$E_{131}B_{35}$	58	195					
$E_{134}B_{19}$	58	152	144	136	165		
$E_{155}B_{76}$	58	221	217		220		280 (57 °C)
$E_{209}B_{45}$	63	208	213			237	215 (57 °C)

[a] Numbers in parentheses specify the annealing temperature. [b] Measured at 10 °C. [c] Sample with deuterated E block. [d] Other conditions: $T_c = 35$ °C, $d = 175$ Å; $T_c = 40$ °C, $d = 180$ Å.

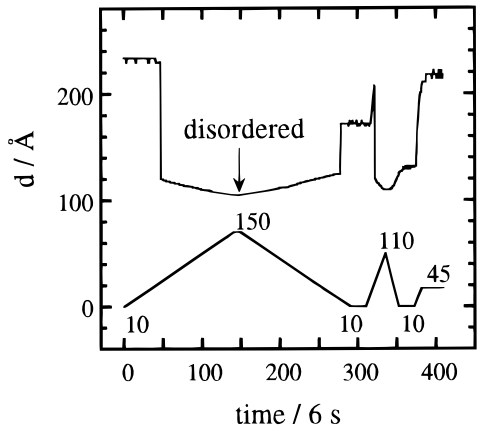

Figure 4. Time series (frames, each 6 s) showing the dominant spacing measured for copolymer $E_{64}B_{60}$ as a function of temperature during the melting and crystallization program indicated. Temperatures (°C) are indicated. The ordered melt has a hexagonal structure. The disordered phase above the ODT is indicated, the spacing being that of the fluctuation (correlation) peak.

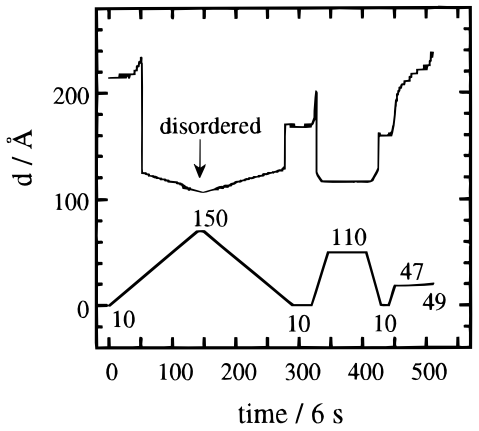

Figure 5. Time series (frames, each 6 s) showing the dominant spacing measured for copolymer $E_{75}B_{54}$ as a function of temperature during the melting and crystallization program indicated. Temperatures (°C) are indicated. The ordered melt has an $Ia\bar{3}d$ structure. The disordered phase above the ODT is indicated, the spacing being that of the fluctuation (correlation) peak.

E blocks have f folds

$$d_f = d_0/(f + 1) \quad (2)$$

Crystal/Liquid-Crystal (CLC) Model. The ND model is inappropriate for copolymers with short B blocks. If the orientation of chains emerging from the crystal end surface is maintained, so as to form an array of B blocks similar to a layer in a smectic liquid crystal, then the maximum lamellar spacing is the extended molecular length, i.e.

$$l_{00} = 0.95z_E + 1.21z_B \quad (3)$$

where the notation l_{00} indicates that neither block is folded, and the equation is written for chains with E blocks in helical conformation and B blocks in trans-planar conformation, z_B being the number of chain atom (C and O atom) in the B-block backbone and 1.21 Å being the length per chain atom along its trans-planar axis (an average value for C−C and C−O bonds).[22] This model was used to explain the Raman spectroscopy of crystalline E_mB_n copolymers with short blocks.[1] Within the CLC model, both E and B blocks may fold, and using the notation l_{fg} to mean the repeat length for chains with f folds in the E block and g folds in the B block, the formula for calculating values of l_{fg} for chains with E blocks in helical conformation and B blocks in trans-planar conformation is

$$l_{fg} = 0.95z_E/(f + 1) + 1.21z_B/(g + 1) \quad (4)$$

Calculation shows that $d_o > l_{00}$ which, since d cannot exceed the extended length of the chain, makes the ND model untenable for unfolded chains.

The constraint on chain conformation in the B layer applies to all crystals, including those with E blocks in folded-chain conformations. The need to maintain normal density is equally important. In many conformations these two requirements are in opposition. In

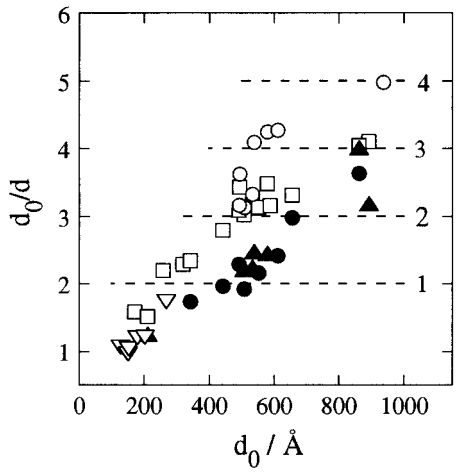

Figure 6. Normal density model. Calculated lamellar spacings for copolymers with unfolded E blocks (d_0, see eq 1) divided by measured lamellar spacings (d) and plotted against d_0. Crystallisation conditions: (□) cooled at 10 °C min^{-1}; (○) quenched; (▲) annealed; (●) self-seeded. The symbol ▽ denotes results from ref 1. The dashed lines indicate the values of d_0/d expected for one to four folds in the E block.

what follows we apply the two models to the present data and then examine the manner in which the system adjusts to meet the two constraints.

Application of the ND model is shown in Figure 6: results obtained previously[1] are included. The data are presented as d_0/d *vs* d_0, thus giving an indication, within the model, of the extent of folding of the E block (see eq 1). Integer folding of the E blocks corresponds to the dashed lines drawn on the diagram labeled 1 to 4. The figure illustrates well the general effect of crystallization conditions, i.e., the systematically higher values of f found for the quenched and cooled samples compared to the self-seeded and annealed samples. Over the data set the difference averages to approximately one fold. It is reasonable to assume that the samples with the fewer folds (self-seeded or annealed) most nearly represent the equilibrium state, which is the focus of present interest. With the possible exception of the region of the diagram enclosing three to four folds, there is no commanding evidence of clustering to the lines representing integer folding; i.e., the data points in this representation are widely scattered. On this evidence alone one might conclude that E-block folding in the copolymers was generally nonintegral.

As explained above, the ND model has no validity for unfolded chains. Moreover the CLC model is conceptually the more satisfactory, since it accommodates the natural orientation of chains which emerge from the end surface of a lamellar crystal. However, in the CLC model comparison of predicted with measured d spacings is not straightforward since, unless the two blocks are equivalently folded, their contributions to the overall lamellar thickness (through eq 4) are not directly related. This point is illustrated in Figure 7a, which shows calculated values of l_{00}/l_{fg} plotted against l_{00}. In constructing the plot only conformations with $f \geq g$ are considered, since the E block has the smaller cross section. Also the trend towards more highly folded conformations at higher values of l_{00} is accommodated by omitting unnecessary points. The dashed lines represent the cases where $f = g$. As can be seen, the effect of variation in copolymer composition is to cause considerable scatter in the data points for all conformations for which $f \neq g$. In other words, the CLC model

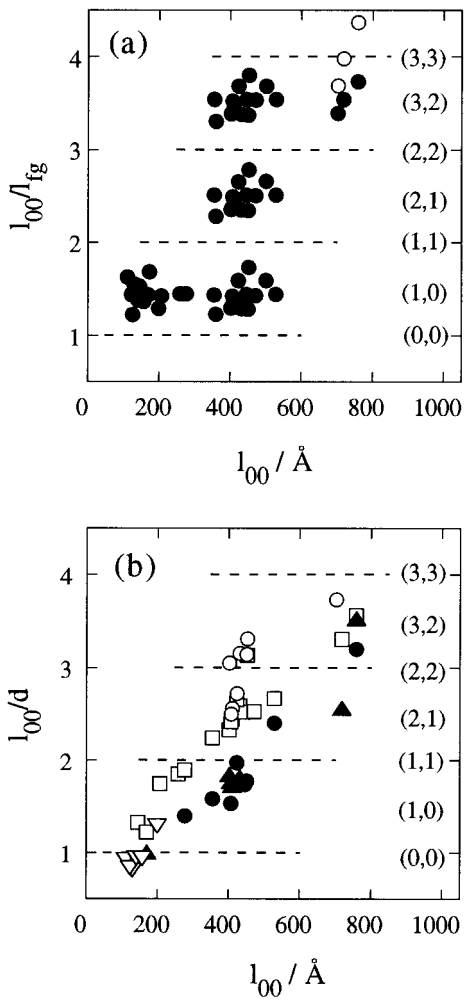

Figure 7. Crystal/liquid-crystal model: (a) Calculated lamellar spacings for copolymers with unfolded E and B blocks (l_{00}, see eq 1) divided by calculated spacings for copolymers with f folds in the E block and g folds in the B block (l_{fg}) and plotted against l_{00}. The values of f and g indicated relate to the dashed lines ($f = g$) and to the filled circles (●, $f = g + 1$). The unfilled circles are for conformation (4,2). (b) Calculated lamellar spacings for copolymers with unfolded E and B blocks (l_{00}) divided by measured lamellar spacings (d) and plotted against l_{00}. Crystallization conditions: (□) cooled at 10 °C min^{-1}; (○) quenched; (▲) annealed; (●) self-seeded. The symbol ▽ denotes results from ref 1. The dashed lines indicate the values of l_{00}/d expected for the conformations with $f = g$ (as indicated).

predicts scatter in the data points, whether plotted in this way or as in Figure 6.

Figure 7b presents the experimental data in the form l_{00}/d plotted against l_{00}, i.e. in a form directly comparable with Figure 7a. The clustering of points away from the (1,1) and (2,2) conformations is in keeping with expectation, since these are ones with the greatest disparity in area of cross-section: see Table 3 for values consistent with the CLC model. Of the conformations considered in Figure 7b, only (2,1), (3,2), and (4,2) have a tolerable match of cross-sectional areas, and thus a tolerable density deficiency within the structure. The effect of this strain in the crystals has been discussed previously with respect to conformations (0,0) and (1,0),[1] and is considered again below.

In itself, Figure 7 does not prove conformity with the CLC model, since the individual data points cannot be readily related between the two plots. However, Figure 7b does enable measured spacings to be assigned to specific conformations, and so to prescribed calculated

Table 3. Areas of Cross Section per Block in Integer-Folded Conformations

conformation	area of cross-section/Å^2		density discrepancy/%
	E-block	B-block	
(0,0)	21	34	38
(1,0)	42	34	19
(1,1)	42	68	38
(2,1)	63	68	7
(2,2)	63	102	38
(3,2)	84	102	12
(3,3)	84	136	38
(4,2)	105	102	3

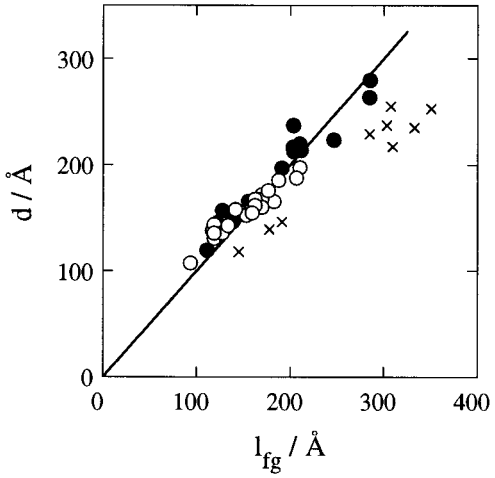

Figure 8. Crystal/liquid-crystal model. Measured lamellar spacing (d) plotted against calculated lamellar spacing l_{fg}, the assignments to a given conformation (f, g) being taken from Figure 7b: (●) annealed or self-seeded samples; (○) cooled or quenched samples. Anomalous samples assigned to conformation (1,0) are denoted (×): see text for details. The 45° line is shown.

spacings for individual copolymers. A comparison of measured d with calculated l_{fg} based on these assignments is shown in Figure 8. Except for the nine copolymers with points lying towards the top of the (1,0) band in Figure 7b (shown as crosses in Figure 8), all the data fit reasonably well to the 45° line. At least some of the scatter of the data in Figure 8 reflects the uncertainty with regard to achievement of equilibrium for a particular state: see Table 2 and related discussion. The anomalous results for the nine copolymers presumably reflect the density problem for the (1,0) conformation, illustrated in Table 3. The finding that the majority of the data points fit rather well to the 45° line in Figure 8, thus removing the scatter inherent in application of the ND model, provides evidence in favor of the CLC model.

The relatively low values measured for d of the nine copolymers could mean that a more-folded conformation, presumably (2,1), formed under kinetic control during crystallization, was not fully annealed out because of the high Gibbs energy of the (1,0) conformation, leading to stacks of mixed lamellae with copolymer chains in different conformations. One possible refinement to the CLC model has not been pursued. It has been shown for other block systems (e.g. oxyethylene/methylene[23]) that a density deficiency can be compensated, at least in part, by tilting one block relative to the other, the overall effect being to reduce the lamellar spacing compared to the collinear structure. The effect could be important for structures in which folded E blocks have a substantially greater area of cross-section than the B blocks, and could explain the anomaly associated with the (1,0) conformation.

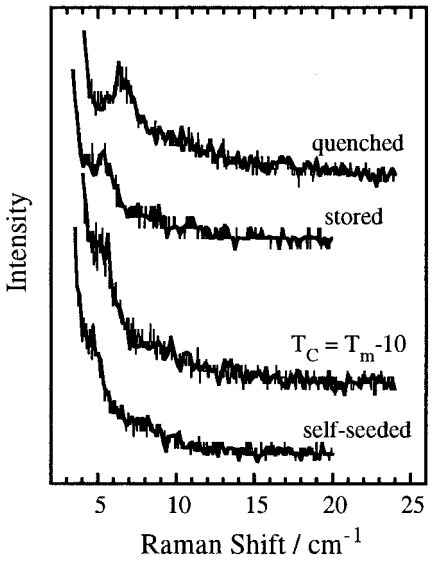

Figure 9. Low-frequency Raman spectra obtained for quenched, stored, crystallized at $T_c = T_m - 10$ °C and self-seeded ($T_c = T_m - 5$ °C) samples of copolymer $E_{76}B_{38}$. The intensity scales and zeros are arbitrary.

Table 4. LAM-1 Frequencies (20 °C) for Crystalline Oxyethylene/Oxybutylene Diblock Copolymers

copolymer	T_m/°C	LAM-1 frequency/cm^{-1}			
		store	quench	$T_c \approx T_m - 10$	self- seeded ($T_c \approx T_m - 5$)
$E_{36}B_{18}$	43	6.2	6.3	6.2	
$E_{43}B_{23}$	47	6.2	6.5	5.7	5.6
$E_{56}B_2$	50	5.2	6.2		4.9
$E_{64}B_{60}$	47	8.0	7.9		7.1
$E_{76}B_{38}$	56	5.4	6.4	5.0	4.5

3.3. Raman Spectroscopy. Selected polymers were examined by Raman spectroscopy: $E_{36}B_{18}$, $E_{43}B_{23}$, $E_{56}B_{27}$, $E_{76}B_{38}$, and $E_{64}B_{60}$. High-frequency spectra were consistent with the E blocks crystallizing in the usual poly(oxyethylene) structure,[20,24,25] the particular indicators used being the bands at 291, 936, and 1231 cm^{-1}.[25] A second indicator, prominent in the low-frequency spectra, was the band at *ca.* 80 cm^{-1} which is assigned to a local mode of the poly(oxyethylene) helix plus a lattice mode of the crystal.[26,27]

Very-low-frequency spectra obtained for copolymer $E_{76}B_{38}$ crystallized under various conditions are shown in Figure 9. The bands at 4−6 cm^{-1} are assigned to the single-node longitudinal acoustic mode (LAM-1). Care was taken in self-seeded crystallization experiments to allow sufficient time for completion of the process (12 h or more, see section 2.5). As can be seen, the LAM-1 frequency depended on crystallization conditions, i.e. ν_1(quenched) > ν_1(high T_c) > ν_1(self-seeded).

Values of the LAM-1 frequency measured for the five copolymers are listed in Table 4. Because of poor definition of peaks (see Figure 9, band widths 2 cm^{-1} or more) spectra were recorded several times in order to improve precision, but even so the uncertainty was probably ±1 cm^{-1}. The frequencies obtained for the well-equilibrated samples (self-seeded or high T_c), together with frequencies obtained previously for shorter chains,[1] are plotted against the reciprocal of l_{fg} in Figure 10, the values of l_{fg} used being determined as discussed above, with preference given to those structures with least density discrepancy. As can be seen, most of the points fit reasonably well to a single straight line through the origin.

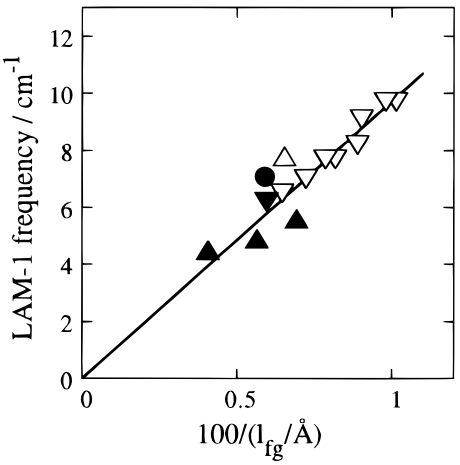

Figure 10. Crystal/liquid-crystal model. LAM-1 frequency plotted against the reciprocal of the calculated lamellar spacing l_{fg}, the assignments to conformations being taken from Figure 7b: (▽, ▼) conformation (0,0); (△, ▲) conformation (1,0); (●) conformation (2,1). Filled symbols indicate results from this work; unfilled symbols indicate results from ref 1. The least-squares straight line through the origin is shown.

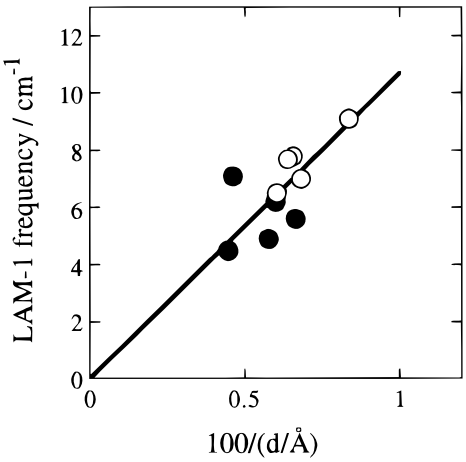

Figure 11. LAM-1 frequency plotted against the reciprocal of the measured lamellar spacing *d*: filled symbols indicate results from this work; unfilled symbols indicate results from ref 1. The least-squares straight line through the origin is shown.

A line (or gentle curve) through the origin of a plot of LAM-1 frequency against reciprocal stem length would be expected for crystalline oligo(oxyethylene)s,[27,28] but is, perhaps, a surprising result for block copolymers. The results for short chains in conformation (0,0) provide strong evidence that this is so, and we accept this regularity in behavior as confirmation of the applicability of the CLC model to the present system, taking the LAM-1 vibration to be that of a composite stem, the E and B components of which have comparable longitudinal force constants.[29] Since in the CLC model any folded conformation contains both overall composite stems and shorter homopolymer stems, the spectra might be expected to contain other LAM-1 bands within them. However, a band at significantly higher wavelength originating from a short stem would have (*via* the Lorentz factor) a relatively low intensity and would not be seen in spectra of the quality shown in Figure 9.

We have explored the possibility that the Raman results can be better fitted by relaxing the restriction of integral folding through a plot of LAM-1 frequency against reciprocal lamellar spacing from SAXS. As shown in Figure 11, fewer data points are available for this plot. Nevertheless it is clear that within experimental error, which impinges equally on the data in Figures 10 and 11, there is no advantage to the broader approach, particularly since it subsumes the CLC model.

3.4. Thermal Analysis. Copolymers subjected to various crystallization procedures were examined by DSC: melting points, T_m, and enthalpies of fusion, $\Delta_{fus}H$, are listed in Table 5.

The DSC curves of quenched samples had broad melting peaks, sometimes splitting into two peaks or showing a shoulder on the main peak. The melting temperatures associated with peaks and shoulders are listed in Table 5 (heating rate of 2 °C min^{-1}). As would be expected from the results of SAXS, examination of samples at different heating rates provided evidence of annealing. For example, crystals formed on quenching copolymer $E_{134}B_{19}$ to 10 °C were unstable at DSC heating rates in the range 1−20 °C min^{-1} (see Figure 12), so much so that they were almost entirely converted to a more stable form (higher melting, T_m = 57 °C) on heating at 1 °C min^{-1}. Crystallization of the same copolymer at 48 and 53 °C, the latter being self seeded, gave the more stable form directly: see Figure 13. The shoulder at high temperature in the DSC curve of the sample crystallized at 53 °C indicates formation of a higher melting form ($T_m \approx$ 58 °C), probably a less-folded structure. In support of this assignment, the sample taken from storage had a similarly high melting point (see Table 5). Melting peaks at abnormally low temperatures in the DSC curves of certain samples crystallized at high temperatures (self-seeded) gave evidence of fractional crystallization at high temperatures: see, for example, the results for samples $E_{47}B_{62}$, $E_{56}B_{27}$, $E_{64}B_{60}$ and $E_{68}B_{65}$ in Table 5. This effect was not found for samples with E blocks longer than 75 units.

Generally the melting temperatures of samples prepared by self-seeding were higher than those prepared by quenching (see Table 5), a finding which correlates

Table 5. Thermal Analysis of Crystalline Oxyethylene/Oxybutylene Diblock Copolymers[a]

	T_m/°C			$\Delta_{fus}H$/J g^{-1}		
co-polymer	store	quench	self-seeded (T_c/°C)	measured	$\Delta_{fus}H_E$	X_E
$E_{35}B_{12}$	43	42	--	103	161	0.81
$E_{36}B_{18}$	42	40	--	88	160	0.81
$E_{43}B_{23}$	43	41	41, 46	85	159	0.80
$E_{47}B_{62}$	42	42	39, 43	44	139	0.70
$E_{49}B_{9}$	49	49	--	128	166	0.83
$E_{56}B_{27}$	48	46, 47	43, 49	89	159	0.79
$E_{60}B_{29}$	50	--	--	92	165	0.82
$E_{64}B_{60}$	44	44	39, 46	59	149	0.75
$E_{68}B_{65}$	46	46	43, 46	61	156	0.78
$E_{75}B_{54}$	50	50	49, 51	70	153	0.76
$E_{76}B_{38}$	51	48, 50, 52	55−56	89	161	0.79
$E_{85}B_{45}$	52	50, 52	52, 54	85	159	0.79
$E_{96}B_{47}$	58	--	--	90	162	0.79
$E_{100}B_{51}$	52	51, 52	52−53	86	158	0.78
$E_{110}B_{30}$	56	53, 55	52, 57, 58	112	162	0.79
$E_{114}B_{56}$	55	53, 54	53, 56	88	159	0.78
$E_{115}B_{103}$	52	52	53	61	150	0.74
$E_{131}B_{35}$	57	55−56	56, 58, 59	110	158	0.77
$E_{134}B_{19}$	58	55, 57	55, 57, 59	136	167	0.82
$E_{155}B_{76}$	55	54−55	57−58	89	160	0.78
$E_{209}B_{45}$	63	61, 62	63, 65	121	164	0.80

[a] Heating rate = 2 °C min^{-1}. Melting points are corrected for thermal lag: *ca.* −1 °C at 2 °C min^{-1}. Underlining indicates the melting point of the major component. Hyphenation indicates an unresolved broad peak. Values of $\Delta_{fus}H$ are for samples with the highest melting point recorded, either crystallized at high temperature or taken from storage.

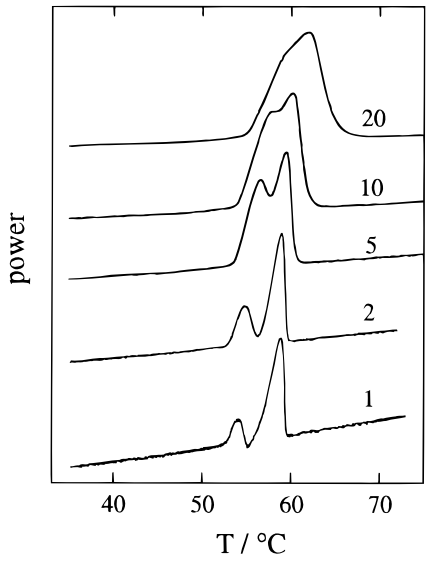

Figure 12. DSC curves for quenched samples of copolymer $E_{134}B_{19}$ and different heating rates (°C min^{-1}) as indicated. The temperature scale is uncorrected. The power scales and zeros are arbitrary.

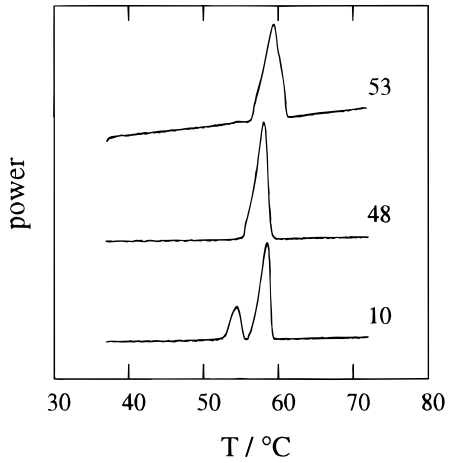

Figure 13. DSC curves for samples of copolymer $E_{134}B_{19}$: quenched to 10 °C, crystallized at 48 °C, and crystallized at 53 °C (self-seeded), as indicated. The temperature scale is uncorrected. The power scales and zeros are arbitrary.

with the shorter *d* spacings of the quenched samples (see Table 2 and Figures 6 and 7b).

We use the DSC curves to extend the information available from SAXS and Raman spectroscopy, finding them particularly useful for those samples which were not investigated in detail by the other techniques. Recognition of an upper limit to the melting point, often across a range of crystallization conditions, is taken as evidence of an equilibrium state. Since SAXS usually yields *d* spacings characteristic of the major component, the recognition of minor components with higher melting points in self-seeded samples of copolymers $E_{85}B_{45}$, $E_{110}B_{30}$, $E_{131}B_{35}$, $E_{134}B_{19}$, and $E_{209}B_{45}$ raises the possibility that their equilibrium states (less-folded states) may not have been achieved in the SAXS experiments. The conditions in the time-resolved SAXS experiments were very different from those of the DSC experiments, not least in the measurement of *d* spacings at low extents of crystallinity, whereas the DSC experiments were necessarily confined to completely crystallized samples. This difference was borne in mind in drawing the conclusions set out in section 4.

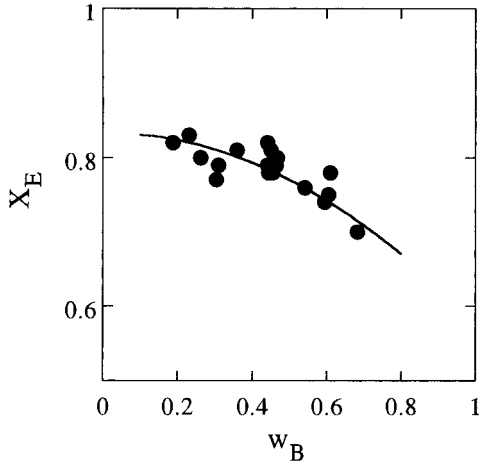

Figure 14. Thermal analysis of E_mB_n block copolymers. Fractional crystallinity of the E block (X_E) *vs* the weight fraction of oxybutylene in the copolymer (w_B).

Measured enthalpies of fusion in J (g of copolymer)$^{-1}$ were converted to J (g of oxyethylene)$^{-1}$ by dividing by the weight fraction of oxyethylene in the copolymer (w_E, see Table 1)

$$\Delta_{fus}H_E = \frac{\Delta_{fus}H}{w_E}$$

and these values were used to calculate the fractional crystallinities of the E blocks (X_E) from

$$X_E = \frac{\Delta_{fus}H_E}{\Delta_{fus}H_E^\circ}$$

where the enthalpy of fusion of perfect crystal is given by[30]

$$\Delta_{fus}H_E^\circ = 175 + 0.650T_m - 0.00253T_m^2$$

As seen in Table 5, values of X_E were remarkably uniform over a wide range of samples, a small downwards trend with increasing B content (see Figure 14, X_E *vs* weight fraction B) being explained by the concomitant increase in the number of folds, with consequent increase in the positive contribution of the surface enthalpy to the enthalpy of the crystalline E layer, hence a decrease in $\Delta_{fus}H_E$. The corresponding plot of melting point (not shown) has scattered data points. Since T_m depends on the entropy as well as the enthalpy of fusion through

$$T_m = \Delta_{fus}H_E/\Delta_{fus}S_E$$

the scatter means that values of $\Delta_{fus}S_E$ were not closely correlated with values of $\Delta_{fus}H_E$. Considering the complexity of the structures under consideration, for both solids and structured liquids, this might be expected.

3.5. Density. The calculations presented in Table 3 indicate a difference between the ND and CLC models in their predictions of bulk density of the noncrystalline component of the lamellae. We have considered this possibility previously for related oxyethylene/ oxypropylene diblock ($E_{40}P_n$) and triblock, ($P_nE_{50}P_n$) copolymers, $n = 1-11$, measuring density discrepancies for the noncrystalline component as high as 4% for lamellar crystals with chains in their unfolded conformation.[3,31] Because of the larger cross-sectional area of the B chain,

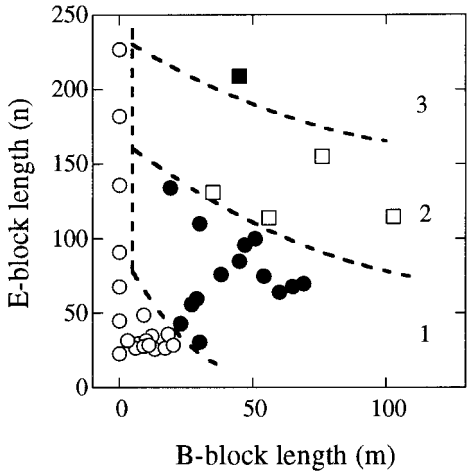

Figure 15. Effect of E and B block lengths on the extent of chain folding of the E block in the equilibrium states of crystalline E_mB_n copolymers: (○) unfolded, (●) one fold, (□) two folds, (■) three folds. The dashed curves approximately delineate the four regions. The data points at $m = 0$ indicate the equilibrium state (unfolded) of low molar mass poly(oxyethylene)s.

the effect should be larger for E_mB_n copolymers. Unfortunately, it was not possible to make such measurements in the present study. Simple flotation and gradient tube methods are ruled out as the solubilities of the two components are so different: E_m is soluble in water; B_n is soluble in practically every organic solvent. The picnometric method used previously is experimentally demanding[3] and is a possibility for the future.

4. Summary and Conclusions

It must be stressed that the normal density (ND) and crystal/liquid-crystal (CLC) models represent two ideal lamellar structures. The likelihood is that the structures of the real crystalline E_mB_n copolymers fall between these two extremes. Both the ND and CLC models describe the data well for the longer copolymers. However, the evidence presented in this paper favors the CLC model, particularly so for the shorter copolymers. This model satisfactorily describes the structures of both quenched and self-seeded/annealed copolymers, the latter having fewer folds.

As would be expected, the extent of folding in the copolymers increases with length of both E and B blocks. This effect is summarized in Figure 15, which relates the extent of folding in the E block in the equilibrium state to the E and B block lengths of the copolymer. The diagram is based on Figure 7b, but also takes into account findings from DSC, as discussed in section 3.4. Buckley and Kovacs[32] have demonstrated the unfolded equilibrium state of polyethylene glycols with chain lengths up to E_{227} ($M_n \leq 10\,000$ g mol^{-1}), and these poly(oxyethylene)s are represented as data points on the $m = 0$ axis. The positioning of the boundaries between the regions of different extents of folding of the E block, shown as dashed lines in Figure 15, is speculative, not least because of uncertainty in assignments (discussed in section 3). Nevertheless the diagram allows useful prediction of the state of E-block folding in the E_mB_n system.

Acknowledgment. Thanks are due to Dr. G.-E. Yu for invaluable help with the syntheses of the copolymers and to Dr. F. Heatley and Mr. K. Nixon for help with their characterization by NMR and GPC. Financial support came from the Engineering and Physical Science Research Council (U.K.). S.M.M. is particularly grateful for an ORS award and a University of Manchester Scholarship. Finally we thank our reviewer for careful reading of the manuscript and stimulating comments which have led to improvements in our presentation and discussion.

References and Notes

(1) Yang, Y.-W.; Tanodekaew, S.; Mai, S.-M.; Booth, C.; Ryan, A. J.; Bras, W.; Viras, K. *Macromolecules* **1995**, *28*, 6029.
(2) Ryan, A. J.; Fairclough, J. P. A.; Hamley, I. W.; Mai, S.-M.; Booth, C. *Macromolecules* **1997**, *30*, 1723.
(3) Ashman, P. C.; Booth, C. *Polymer* **1975**, *16*, 889.
(4) DiMarzio, E. A.; Guttman, C. M.; Hoffmann, J. D. *Macromolecules* **1980**, *13*, 1194.
(5) Whitmore, M. D.; Noolandi, J. *Macromolecules* **1988**, *21*, 1482.
(6) Vilgis, T; Halperin, A. *Macromolecules* **1991**, *24*, 2090.
(7) Galin, M.; Mathis, A. *Macromolecules* **1981**, *14*, 677.
(8) Gervais, M.; Gallot, B. *Makromol. Chem.* **1973**, *171*, 157; **1977**, *178*, 1577.
(9) Nojima, S.; Kato, K.; Yamamoto, S.; Ashida, T. *Macromolecules* **1992**, *25*, 2237.
(10) Rangarajan, P.; Register, R. A.; Fetters, L. J. *Macromolecules* **1993**, *26*, 4640.
(11) Rangarajan, P.; Register, R. A.; Adamson, D. H.; Fetters, L. J.; Bras, W.; Naylor, S.; Ryan, A. J. *Macromolecules* **1995**, *28*, 1422.
(12) Ryan, A. J.; Hamley, I. W.; Bras, W.; Bates, F. S *Macromolecules* **1995**, *28*, 3860.
(13) Hamley, I. W.; Fairclough, J. P. A.; Terrill, N. J.; Ryan, A. J.; Lipic, P. M.; Bates, F. S.; Towns-Andrews, E. *Macromolecules* **1996**, *29*, 8835.
(14) Mai, S.-M.; Fairclough, J. P. A.; Hamley, I. W.; Denny, R. C.; Matsen, M.; Liao, B.-X.; Booth, C.; Ryan, A. J. *Macromolecules* **1996**, *29*, 6212.
(15) Bras, W.; Derbyshire, G. E.; Ryan, A. J.; Mant, G. R.; Felton, A.; Lewis, R. A.; Hall, C. J.; Greaves, G. N. *Nucl. Instrum. Methods Phys. Res.* **1993**, *A326*, 587.
(16) Ryan, A. J. *J. Therm. Anal.* **1993**, *40*, 887.
(17) Bras, W.; Derbyshire, G. E.; Clarke, S.; Devine, A.; Komanschek, B. U.; Cooke, J.; Ryan, A. J. *J. Appl. Crystallogr.* **1994**, *35*, 4537.
(18) Ryan, A. J.; Bras, W.; Mant, G. R.; Derbyshire, G. E. *Polymer* **1994**, *35*, 4537.
(19) Viras, K.; King, T. A.; Booth, C. *J. Polym. Sci., Polym. Phys. Ed.* **1985**, *23*, 471.
(20) Takahashi, Y.; Tadokoro, H. *Macromolecules* **1973**, *6*, 881.
(21) Craven, J. R.; Zhang, H.; Booth, C. *J. Chem. Soc., Faraday Trans.* **1991**, *87*, 1183.
(22) Flory, P. J. *Statistical Mechanics of Chain Molecules*; Interscience: New York, 1969; p 165.
(23) (a) Domszy, R. C.; Booth, C. *Makromol. Chem.* **1982**, *183*, 1051. (b) Teo, H. H.; Swales, T. G. E.; Domszy, R. C.; Heatley, F.; Booth, C. *Makromol. Chem.* **1983**, *184*, 861. (c) Swales, T. G. E.; Domszy, R. C., Beddoes, R. L.; Price, C.; Booth, C. *J. Polym. Sci., Polym. Phys. Ed.* **1985**, *23*, 1585.
(24) Koenig, J. L.; Angood, A. C. *J. Polym. Sci., Part A-2* **1970**, *8*, 1787.
(25) Matsuura, H.; Fukuhara, K. *J. Phys. Chem.* **1987**, *91*, 6139.
(26) Rabolt, J. F.; Johnson, K. W.; Zitter, R. N. *J. Chem. Phys.* **1974**, *61*, 504.
(27) Viras, K.; Teo, H. H.; Marshall, A.; Domszy, R. C.; King, T. A.; Booth, C. *J. Polym. Sci., Polym. Phys. Ed.* **1983**, *21*, 919.
(28) Campbell, C.; Viras, K; Booth, C. *J. Polym. Sci., Polym. Phys. Ed.* **1991**, *29*, 1613.
(29) Hsu, S. L.; Ford, G. W.; Krimm, S. *J. Polym. Sci., Polym. Phys. Ed.* **1977**, *15*, 1769.
(30) Campbell, C.; Viras, K.; Richardson, M. J.; Masters, A. J.; Booth, C. *Makromol. Chem.* **1993**, *194*, 799.
(31) Ashman, P.; Booth, C.; Cooper, D. R.; Price, C. *Polymer* **1975**, *16*, 897.
(32) Buckley, C. P.; Kovacs, A. J. *Prog. Colloid Polym. Sci.* **1975**, *58*, 44.

MA971158F